Materials Chemistry and Physics 292 (2022) 126792

Contents lists available at ScienceDirect

Materials Chemistry and Physics

journal homepage: www.elsevier.com/locate/matchemphys

Hyperbranched amino modified magnetic nanoparticles for simultaneous removal of heavy metal ions from aqueous solutions

V.P. Kothavale [a,b], A. Sharma [c], R.P. Dhavale [d], V.D. Chavan [e], S.R. Shingte [a], O. Selyshchev [c], T.D. Dongale [e], H.H. Park [d], D.R.T. Zahn [c], G. Salvan [c], P.B. Patil [a,*]

[a] Department of Physics, The New College, Shivaji University, Kolhapur, Maharashtra, 416012, India
[b] Department of Physics, Bhogawati Mahavidyalaya, Kurukali, Shivaji University, Kolhapur, Maharashtra, 416012, India
[c] Semiconductor Physics, Chemnitz University of Technology, 09107, Chemnitz, Germany
[d] Department of Materials Science and Engineering, Yonsei University, 50 Yonsei-ro, Seodaemun-gu, Seoul, 03722, South Korea
[e] School of Nanoscience and Technology, Shivaji University Kolhapur, Maharashtra, 416004, India

HIGHLIGHTS

- MNPs of 8.6 ± 1.5 nm size with pure magnetite phase synthesized by a thermal decomposition method.
- MNP-PAMAM nanoadsorbents prepared by modifying MNPs with the PAMAM dendrimer to simultaneously remove HMIs.
- Simultaneous maximum adsorption capacities for Pb(II), Ni(II), and Cd(II) are 37, 32, and 25 mg/g respectively.
- The adsorption kinetics and isotherm follow Langmuir and pseudo-second-order models, respectively.
- The MNP-PAMAM nanoadsorbents exhibited good regeneration performance.

GRAPHICAL ABSTRACT

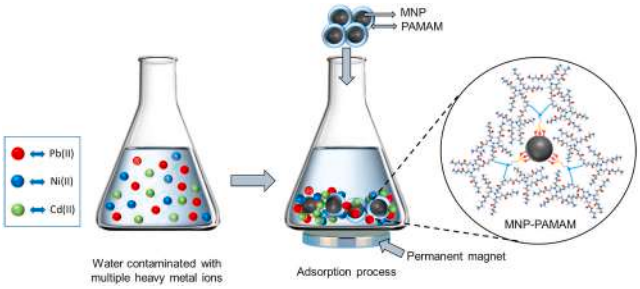

ARTICLE INFO

Keywords:
Magnetic nanoparticles (MNPs)
Functionalization
PAMAM dendrimer
Adsorption
Simultaneous removal

ABSTRACT

Functionalized magnetic nanoparticles (MNPs) are gaining considerable interest to remove heavy metal ions (HMIs) from polluted water. However, simultaneous removal of coexisting HMIs remains a challenge due to the competition between different HMIs to bind the limited number of adsorption sites of the adsorbent. To address this, abundant adsorption sites were provided by increasing the density of functional groups on the surface of MNPs using the second-generation of a hyperbranched polyamidoamine (PAMAM) dendrimer. For dendritic modification, a novel approach was used to remove the surfactant coating on the as-prepared MNPs synthesized by the thermal decomposition. The magnetic nanoadsorbents were extensively characterized by XRD, TEM, FTIR, zeta potentials, XPS, SQUID-VSM, and BET. The MNP-PAMAM nanoadsorbents were utilized for the simultaneous removal of model HMIs Pb(II), Ni(II), and Cd(II) from aqueous solutions by batch adsorption experiment. Pb(II), Ni(II), and Cd(II) were found to have maximum adsorption capacities (q_m) of 37.00, 31.92, and 24.94 mg/g, respectively, in the ternary system and 92.82, 80.10, and 57.72 mg/g, respectively in single systems. The adsorption kinetics and isotherm follow Langmuir and pseudo-second-order models, respectively. MNP-PAMAM

* Corresponding author.
E-mail address: prashantphy@gmail.com (P.B. Patil).

https://doi.org/10.1016/j.matchemphys.2022.126792
Received 11 May 2022; Received in revised form 31 August 2022; Accepted 15 September 2022
Available online 20 September 2022

nanoformulation developed in this study can also be useful in other applications such as biomedical, sensors, and nanocatalysis.

1. Introduction

Rapid urbanization and industrial development have led to water pollution by toxic heavy metal ions (HMIs) and it is of utmost importance to develop an effective method to purify such effluent water. Many technologies have been explored to remove HMIs from polluted water. Still, adsorption holds the edge due to easy operation, efficient removal, and cost-effectiveness. Presently, various adsorbents such as activated carbon [1], biomaterials [2], zeolite [3], graphene-based materials [4], and magnetic nanoparticles (MNPs) [5] have been investigated. Among these adsorbents, MNPs are promising due to the possibility of tailoring MNPs surfaces to have a high binding affinity towards HMIs. In addition to this, the high specific surface area and good colloidal stability of MNPs are beneficial for a higher adsorption capacity (q_e). Furthermore, MNPs can be separated from wastewater using a magnet and reused after desorbing the adsorbed HMIs. To improve metal q_e, MNPs were surface functionalized to provide specific adsorption sites like –COOH, $–NH_2$, –OH, –SH [5]. For this, different materials such as polyacrylic acid (PAA) [6], chitosan [7], meso-2,3-dimercaptosuccinic acid [8,9] gum arabic [10], (3-aminopropyl)triethoxysilane (APTES) [11], (3-aminopropyl)triethoxysilane-glutaraldehyde [12], and polyvinyl acetate-iminodiacetic acid [13] were used to modify the surface of MNPs. Notwithstanding these efforts, the MNP-based adsorbents still suffer from one major problem: low q_e for coexisting multiple types of HMIs. In fact, contaminated water originating from many industrial activities consists of several toxic HMIs that exist together. With multiple HMIs, there will be a competition between different HMIs to bind to the limited number of adsorption sites. This limitation arises due to the low density and inhomogeneous distribution of adsorption sites on adsorbents surfaces.

To overcome the limitation in simultaneous removal of multiple HMIs, we propose to increase the density of the functional groups by modifying the MNPs surface by the second-generation of a hyperbranched polyamidoamine (PAMAM) dendrimer. PAMAM dendrimer is a class of hyperbranched long-chain macromolecules consisting of three basic units with an initial core, repeating units, and terminal units. The synthesis of amine-terminated PAMAM dendrimers is carried out in two steps [14]. In the first step, a Michael addition reaction of amino groups to methyl acrylate is performed. The second step involves amidation of the resulting methyl ester with ethylenediamine. To prepare higher generations of the dendrimer, the steps of addition-amidation reactions are repeated. The density of functional groups increases after the synthesis of each generation of PAMAM. The first generation of PAMAM dendrimer contains 8 amine groups, while the second generation contains 16 amine groups that are available as adsorption sites. Due to the higher density of adsorption sites, MNPs modified with second-generation PAMAM could serve as an effective nanoadsorbent for simultaneous removal of multiple HMIs from contaminated water.

In many applications such as biomedical and catalysis, including HMIs removal, highly stable, non-agglomerated, and monodispersed MNPs are a prerequisite. High temperature synthesis using oleic acid (OA) and oleylamine (OM) surfactant/capping agent has been the most widely used method for obtaining such MNPs [15]. However, the coating of surfactants remains on the MNPs surface after high temperature synthesis. The presence of such coating leads to aggregation and also obscures further functionalization processes. To modify with the PAMAM dendrimer, MNPs first need to be functionalized with amine groups prior to the addition-amidation reactions. In general, for dendritic modification of MNPs, the residual coating needs to be completely exchanged for dispersants with irreversible affinity to the MNPs surface. Therefore, for dendritic modification, MNPs prepared by a surfactant-free approach have always been used [16]. There are few reports which uses PAMAM dendrimer modified MNPs as adsorbent materials for HMIs removal where MNPs were prepared with surfactant free approach [17,18]. However, this approach loses the benefits of controlled synthesis of MNPs prepared using surfactant/capping agents, which provide reproducible and highly uniform physicochemical characteristics. To address this issue, in this work, OA/OM moieties on the surface of MNPs were removed by repeated recrystallization of MNPs by refluxing in a methanol/hexane solvent mixture to get purified MNPs. The purified MNPs were amino-functionalized by the strategy of monolayer grafting of APTES as in our previous report [19]. These APTES functionalized MNPs were modified with second-generation PAMAM. The present work is the first report wherein the OA/OM coated MNPs surface has been modified with second generation dendrimer. The MNP-PAMAM nanoadsorbents were employed for the individual and simultaneous adsorption study of the Pb(II), Cd(II), and Ni (II) HMIs from an aqueous solution.

2. Materials and methods

2.1. Chemicals

All of the chemicals used were of analytical grade and were used as they were received. Ferric acetylacetonate ($Fe(acac)_3$), 1,2-Octanediol, (3-aminopropyl)triethoxysilane (APTES), methyl acrylate, and ethylenediamine were obtained from Sigma Aldrich. Diphenyl ether (DPE), dibenzyl ether (DBE), oleic acid (OA), oleylamine (OM), dimethyl sulfoxide (DMSO), hexane, lead nitrate, cadmium sulfate, methanol, toluene, and ethanol were bought from S D Fine-Chem India. Nickel (II) sulfate and hydrochloric acid were acquired from Thomas Baker. The pH buffer tablets (3–9) were supplied by Thermo Fisher Scientific.

2.2. Synthesis of MNPs

The monodispersed Fe_3O_4 MNPs were synthesized by the thermal decomposition method with a slight modification of an earlier report [20]. In this work a bisolvent system of DPE and DBE was used. Initially, 1:1 ratio of DPE (10 ml) and DBE (10 ml) were mixed in a three-necked flask of volume 250 mL. To this, OA (6 mmol) and OM (12 mmol) were slowly added with vigorous stirring. While continuing the stirring, Fe $(acac)_3$ (2 mmol) and 1,2-octanediol (10 mmol) were mixed into the reaction mixture. Under an argon atmosphere, the resulting reaction mixture was heated to 200 °C in the heating mantle for 2 h and then refluxed at 280 °C for 1 h. The resulting black coloured solution was allowed to cool down to room temperature (RT) and the supernatant was discarded. By magnetic decantation, the synthesized nanoparticles were first washed with ethanol and then washed five times with a 1:1 mixture of ethanol and hexane to remove excess ligands [21]. The resultant MNPs were dried in a vacuum desiccator.

2.3. Preparation of dendrimer modified MNPs

Before surface modification, the coating of OA and OM from the surface of as-prepared MNPs was removed to obtain purified MNPs. For this, 1.5 gm MNPs were added to 150 mL methanol/hexane (1:1) solvent and refluxed three times at 65 °C for 1 h under argon atmosphere [22]. The purified MNPs were functionalized by APTES using a method reported by us with slight modification [19,23]. Briefly, 1.5 gm of MNPs were dispersed in the 300 mL methanol/toluene (1:1) mixture by an ultrasonicator. This solution was heated at 95 °C till the volume is reduced to 150 mL. The volume was adjusted to 300 mL by adding

methanol into the solution. This procedure was repeated two more times to make the solution anhydrous. After adding 9 mL APTES, the above solution was shaken for 24 h at 70 °C. The resultant solution was cooled to RT to get APTES functionalized MNPs (MNP-APTES). Then MNP-APTES were washed three times with ethanol. The synthesized MNP-APTES were identified as generation zero dendrimer (MNP-G0). The MNP-G0 was further modified by the PAMAM dendrimer through the Michael addition and amidation reaction [24,25]. In brief, 1.5 gm MNP-G0 was dispersed in 50 mL methanol. To this, 20 mL methyl acrylate was added slowly. The resulting solution was sonicated for 7 h at RT. The product was washed five times with methanol, dried in a vacuum desiccator and named MNP-G0.5. The MNP-G0.5 was dispersed in 20 ml methanol and 4 mL ethylenediamine was added dropwise. Then the mixture was shaken for 3 h at RT. The product was washed five times with methanol to obtain the first-generation dendrimer MNPs (MNP-G1). The MNP-G1.5 and second-generation dendrimer MNPs (MNP-G2) were prepared by repeating the above procedure. In this work, the resultant second-generation MNPs are identified as MNP-PAMAM. The schematic representation of the modification of MNPs by amino terminated second-generation PAMAM dendrimer (MNP-PAMAM) is presented in Scheme 1.

2.4. Characterization

The X-ray diffraction (XRD) measurements were performed on a SmartLab X-ray diffractometer from Rigaku equipped with a rotating copper anode using Cu-K_α (0.154 nm) in the range of 20°–100°. The XRD diffraction data were analyzed by the FullProf program using the Rietveld refinement technique. A Tecnai G2 STwin model transmission electron microscope (TEM) operated at a voltage of 200 kV was used to record the micrographs, particle size, shape, and for microstructural investigations. Fourier transform infrared (FTIR) spectra of samples were obtained using a Jasco 4600 FTIR spectrometer using the KBr pellet technique. The zeta potentials of nanoadsorbents were measured by a Malvern Instruments Zetasizer Nano ZS90. X-ray photoelectron spectroscopy (XPS) was performed for the chemical analysis using an ESCALAB 250Xi photoelectron spectrometer from Thermo Scientific equipped with a monochromatic Al K_α ($h\nu = 1486.68$ eV) X-ray source. The superconducting quantum interference device vibrating sample magnetometry (SQUID-VSM) from Quantum Design was used to investigate the magnetic properties of samples. Zero field-cooled (ZFC) and field-cooled (FC) magnetization measurements were taken in the temperature range between 2 K and 400 K with 100 Oe applied magnetic field. The N_2 adsorption and desorption isotherm technique was used to measure the specific surface area by Brunauer-Emmett-Teller (BET) on the Quantachrome Instruments v10.0. The concentration of HMIs was measured using a Thermofisher AA203 atomic absorption spectrometer.

2.5. Batch adsorption experiment

The batch adsorption experiment was carried out at RT to study the individual and simultaneous adsorption behaviour of Pb(II), Cd(II), and Ni(II) HMIs on MNP-PAMAM nanoadsorbent in aqueous solutions. In the batch adsorption experiment, the parameters like pH, adsorbent dose, contact time, and initial concentration of HMIs were optimized. The detailed variation of parameters in the batch adsorption experiment are given in Table S1 of supplementary material. Typically, a known amount of MNP-PAMAM was added in a 50 mL aqueous solution of HMIs in a 100 mL Erlenmeyer flask. The mixture was shaken in an incubator shaker at 150 rpm for a specific time for better interaction between HMIs and nanoadsorbent surface to attain the adsorption equilibrium. After adsorption, the HMIs loaded MNP-PAMAM was separated from the aqueous solutions by magnetic decantation and the remaining concentration of HMIs were measured by AAS. The following equations calculate the removal efficiency (R) and the q_e of nanoadsorbent for HMIs.

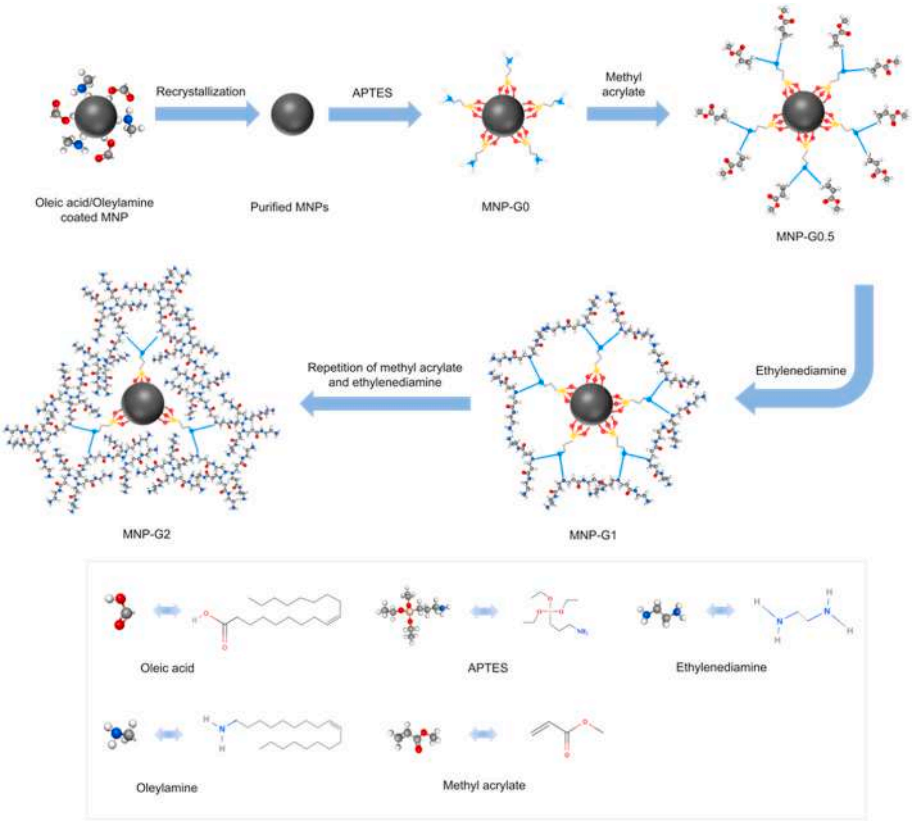

Scheme 1. Stepwise surface modification of as-prepared MNPs by second-generation amine-terminated PAMAM dendrimer (MNP-G2).

$$R(\%) = \frac{C_0 - C_e}{C_o} \times 100 \quad (1)$$

$$q_e = \frac{(C_0 - C_e)\, V}{m} \quad (2)$$

where.

C_0 = Initial HMIs concentration (mg/L).

C_e = Final HMIs equilibrium concentration (mg/L).

V= Volume of HMIs solution (mL) and

m = Mass of the nanoadsorbent used (mg).

The reusability of MNP-PAMAM was studied by performing the adsorption-desorption experiments up to five successive cycles. For the desorption experiment the nanoadsorbent was first loaded with Pb(II), Cd(II), or Ni(II) HMIs. For the desorption of adsorbed ions, the loaded MNP-PAMAM was suspended in 25 ml 0.1 M HCl solution as a desorption agent and shaken for 120 min to reach desorption equilibrium. Then nanoadsorbents were isolated magnetically, washed with double distilled water, and dried to reuse for the next adsorption cycle.

3. Results and discussion

3.1. Characterizations of MNP-PAMAM nanoadsorbents

Rietveld refinement was performed to analyze the XRD data of the MNPs and MNP-PAMAM (Fig. 1A). The magnetite phase (Fe_3O_4) is revealed by the presence of diffraction peaks corresponding to a cubic lattice system with space group Fd-3m (JCPDS card No. 00-019-0629). No other peaks due to phase impurities were observed, indicative of the pure magnetite phase. The average crystallite size of the MNPs was calculated from the Debye Scherrer equation [26] and found to be 8.33 nm. The modification of MNPs by PAMAM did not change the characteristic XRD pattern. The refined lattice parameters after Rietveld fitting of diffraction spectra of MNPs and MNP-PAMAM are tabulated in Table S2. The shape, size, and microstructure of MNPs were studied by TEM (Fig. 1B). MNPs of almost spherical shape with relatively uniform size distribution can be seen. The particle size distribution (Fig. S1) was obtained by analysing multiple TEM micrographs and the average size of MNPs was (8.6 ± 1.5) nm. The diffraction rings in the electron diffraction pattern of MNPs (inset in Fig. 1B) are indexed to the cubic structure of the magnetite phase, which corroborates the XRD analysis. The rings in the electron diffraction of the MNPs consist of small spots indicating their polynanocrystalline nature. The TEM micrograph of MNP-PAMAM with inset showing the electron diffraction is shown in Fig. S2.

The FTIR analysis was performed to elucidate each step of the surface modification of MNPs by the PAMAM dendrimer. Fig. 2 shows the FTIR spectra of MNPs (a), MNP-APTES (b), MNP-G0.5 (c), MNP-G1.0 (d), MNP-G1.5 (e), and MNP-G2.0 (f). In all spectra, strong absorption peaks around 585 and 628 cm^{-1} corresponding to the Fe–O bond of iron oxide can be observed [27]. In as-prepared MNPs spectra, the peak at 1030 cm^{-1} corresponds to the C–O single bond stretching and the peaks at 2852 and 2922 cm^{-1} due to symmetric and asymmetric vibration of the CH_2 bands reveal the chemisorption of OA [8,28,29]. The region of

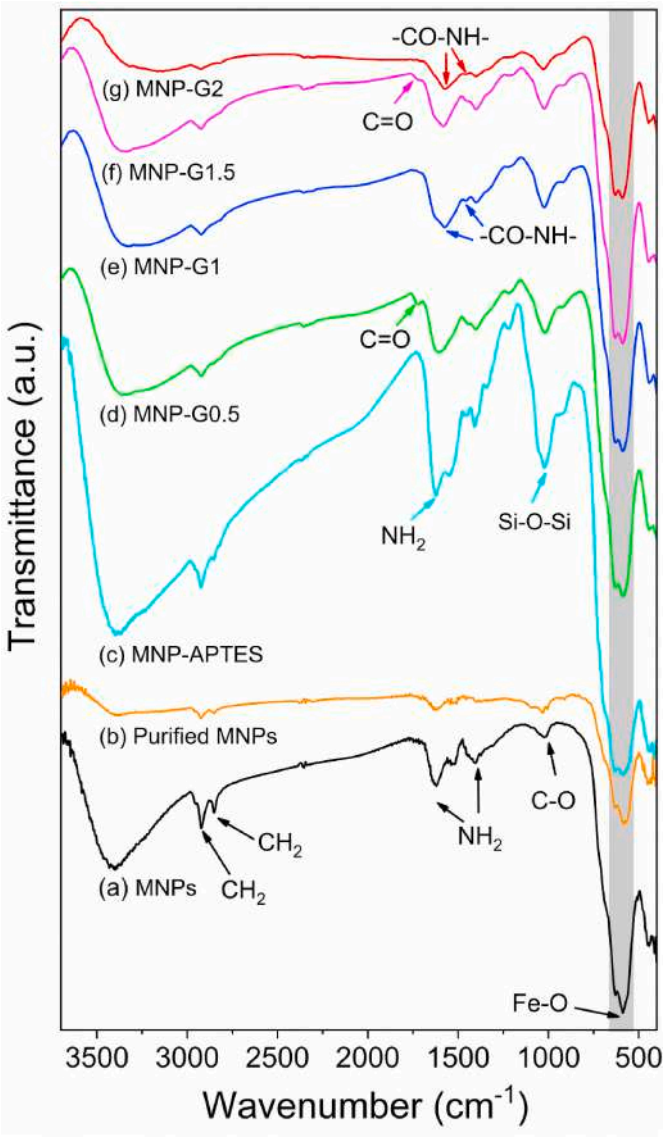

Fig. 2. FTIR spectra of (a) as prepared MNPs, (b) purified MNPs, (c) APTES functionalized MNPs (MNP-G0), (d) half-generation dendrimer (MNP-G0.5), (e) first-generation dendrimer (MNP-G1.0), (f) one and half-generation dendrimer (MNP-G1.5), and (g) second-generation dendrimer (MNP-G2.0).

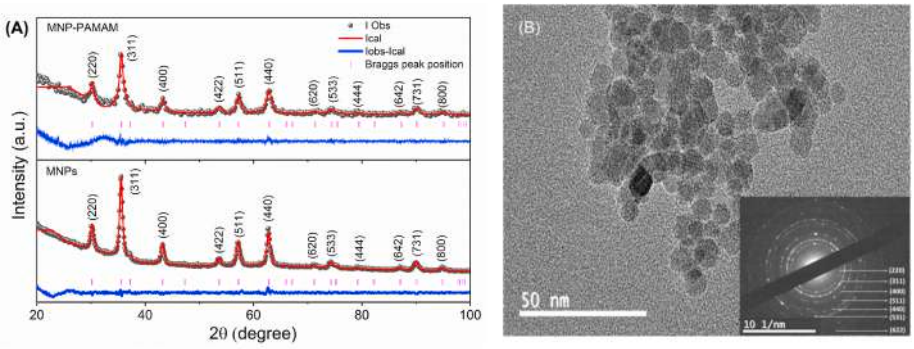

Fig. 1. (A) XRD patterns of MNPs and MNP-PAMAM with corresponding Rietveld refinement profile using the Fullprof program. (B) TEM micrograph and electron diffraction pattern (inset) of MNPs.

1405–1602 cm^{-1} is assigned to the NH_2 bending mode of OM [30]. This proves that the surface of the as-prepared MNPs is chemisorbed by OA and OM moieties. After purification of as-prepared MNPs by refluxing in a methanol/hexane solvent, the characteristic C–O peak (1030 cm^{-1}) and CH_2 peaks (2852 and 2922 cm^{-1}) correspond to OA and NH_2 band (1405-1602 cm^{-1}) due to OM were remarkably decreased (Fig. 2b). This result reveals that the OA and OM moieties were removed from the surface of as-prepared MNPs, with few traces remaining. The spectrum shown in Fig. 2c confirms the functionalization of APTES on the surface of the MNPs. The broad peak at 1024 cm^{-1} corresponds to the Si–O–Si group of APTES [12]. Moreover, the strong peak at 1621 cm^{-1} can be attributed to the NH_2 bending mode of the APTES. In the half generations spectra (MNP-G0.5 and MNP-G1.5), the presence of ester groups from methyl acrylate is established from the C═O stretching vibrations at 1721 cm^{-1}. The most interesting aspect of the full generation dendrimer spectra (MNP-G1.0 and MNP-G2.0) is the disappearance of C═O stretching and the presence of –CO–NH- bonds demonstrating the successful amidation [16,25,31,32]. The FTIR investigation confirms the stepwise modification of the MNPs surface by the PAMAM dendrimer.

The XPS investigation was performed to analyze the elemental composition and chemical states of as-prepared MNPs and MNP-PAMAM. The XPS survey spectra of the MNPs and MNP-PAMAM shows the presence of iron, oxygen, and carbon (Fig. 3A). In the survey spectra of MNP-PAMAM, the presence of silicon implies the APTES on the surface of MNPs and the N 1s peak indicates the modification of MNPs by PAMAM. The Fe 2p core-level XPS spectrum of MNP-PAMAM (Fig. 3B) shows two main peaks. These two peaks of Fe $2p_{1/2}$ (724.86 eV) and Fe $2p_{3/2}$ (711.76 eV) states are characteristic peaks of Fe_3O_4. Furthermore, these Fe 2p core-level spectra can be deconvoluted into Fe^{2+} peaks (Fe $2p_{3/2}$: 711.26 eV, Fe $2p_{1/2}$: 724.56 eV and satellite: 719.76 eV) and Fe^{3+} peaks (Fe $2p_{3/2}$: 714.66 eV, Fe $2p_{1/2}$: 727.86 eV and satellite: 732.66 eV) suggesting a mixed-valence state of Fe ions in Fe_3O_4 [33,34]. The deconvolution of the Si 2p spectrum (Fig. 3C) into two peaks at 98.16 eV and 101.76 eV assigned to Si–C and Si–O bonds, respectively, indicates the successful grafting of APTES on the surface of MNPs [35]. A lone broad peak located at 399.9 eV in the high-resolution spectrum of N 1s (Fig. 3D) is due to the amino groups (–NH_2) of the PAMAM structure [36]. Overall, the XPS and FTIR investigations confirm the successful surface modification of MNPs by the PAMAM dendrimer.

To study the surface charge and colloidal stability of the MNP-PAMAM, zeta potential measurements were carried out in pH range 3–10 (Fig. 4). The isoelectric point (IEP) or pH corresponding to zero zeta potential was found to be 8.3. The MNP-PAMAM has a positive surface charge at pH < IEP and a negative surface charge at pH > IEP. At lower pH, NH_2 groups convert to NH_3^+, while positive charge gradually decreases with increased pH [24]. The zeta potential values around neutral pH demonstrate good colloidal stability due to electrostatic repulsion among the MNP-PAMAM nanoadsorbents [37]. The observed zeta potential and IEP values are in agreement with the literature [24,

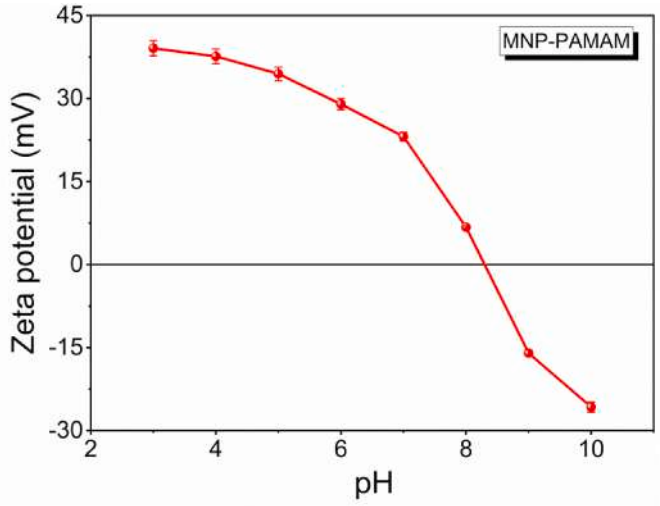

Fig. 4. Effect of pH on the zeta potential of the MNP-PAMAM nanoadsorbent prepared by modifying the MNPs with the second-generation dendrimer.

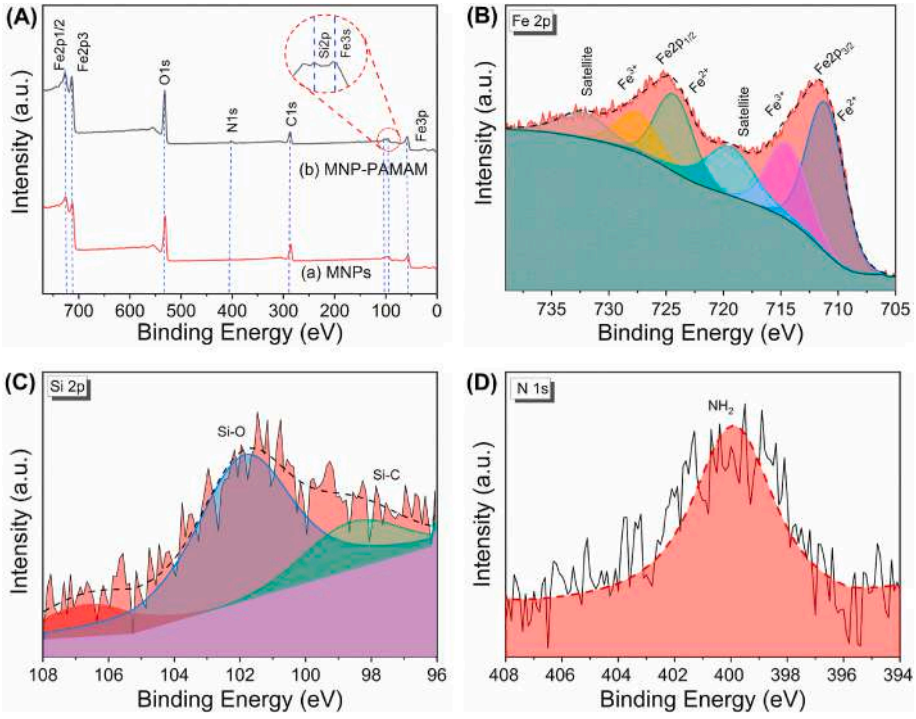

Fig. 3. (A) XPS survey spectra of MNPs (a) and MNP-PAMAM (b). Deconvoluted XPS spectra of (B) Fe 2p and (C) Si 2p of MNP-PAMAM. (D) High-resolution XPS spectrum of N 1s of MNP-PAMAM.

35].

The SQUID-VSM measured magnetization hysteresis loops of as-prepared MNPs and MNP-PAMAM recorded at 300 K (RT) are shown in Fig. 5A. The nonsaturating magnetization along with zero coercivity and remanence at RT suggests that both the as-prepared MNPs and MNP-PAMAM reveals superparamagnetic nature [19]. The saturation magnetization (M_s) of MNPs at RT is 69 emu/g. After surface modification of MNPs by PAMAM, the M_S value decreased to 64 emu/g. As the temperature was lowered to 10 K, the MNPs displayed a hysteresis loop with a coercivity of 176 Oe (Inset Fig. 5A). The magnetization against temperature curves under ZFC and FC conditions for the MNPs measured at 100 Oe magnetic field are shown in Fig. 5B. The blocking temperature, T_B = 137 K, indicates that the MNPs remain in the superparamagnetic state at RT [38]. The average size of MNPs was calculated using the equation "$T_B = VK/25K_B$", where V is the volume of the MNP, K_B is the Boltzmann's constant, and K is the anisotropy constant (1.35×10^4 J/m^3) [39]. Considering the spherical geometry of MNPs, the estimated average particle size of MNPs was ~9.41 nm. This size is comparable with the size calculated from TEM. Furthermore, the grafting percentage of PAMAM dendrimer on the MNPs was calculated from magnetization data [40]. The comparison of M_s values shows that the total amounts of PAMAM dendrimer grafted on the MNPs surface was around 7.24 wt %.

Furthermore, the surface area of the as-prepared MNPs and MNP-PAMAM adsorbents were studied by using the nitrogen adsorption-desorption isotherms (Figs. S3A and B). The surface area of the as-prepared MNPs and MNP-PAMAM were measured by the BET technique. The measured surface areas of as-prepared MNPs and MNP-PAMAM were found to be 75 and 111 m^2/g, respectively. It is worth mentioning that after surface modification of the MNPs by the PAMAM dendrimer, the surface area increased effectively, which is favourable for the improvement of the q_e [41].

3.2. Adsorption studies

3.2.1. Effect of initial pH and adsorbent dose

The solution pH influences the chemistry of HMIs and substantially impacts the ionic state of functional groups of nanoadsorbents in an aqueous medium during the adsorption process [42]. The effect of pH on the q_e of the MNP-PAMAM nanoadsorbents for Pb(II), Cd(II), and Ni(II) HMIs was studied in the pH range from 3 to 9 (Fig. 6A). For Pb(II) and Ni (II), the q_e increased with increasing pH and became maximum at pH 7. For Ni(II), the q_e remained constant after pH 7. In contrast, the q_e for Pb (II) decreased after pH 7 due to a slight precipitation of the aqueous medium. For Cd(II), the q_e reached a maximum at pH 6 and remained constant after that. At low pH (< IEP), the charge on the surface of MNP-PAMAM nanoadsorbents is positive due to the presence of $-NH_3^+$ by the protonation of $-NH_2$ [43]. This leads to the electrostatic repulsion between the protonated surface of nanoadsorbent and contaminant ions, thereby decreasing the uptake capacity of nanoadsorbents. With an increase in pH from 2 to 7, the deprotonation of these groups reduces the repulsion between the MNP-PAMAM and HMIs. Thus it increases the uptake capacity of nanoadsorbents. For convenience, pH 7 was chosen for further adsorption experiments.

The effect of adsorbent dose of MNP-PAMAM on the R and q_e for HMIs was studied (Fig. 6B). The adsorbent dose was varied from 0.02 g/L to 1.0 g/L for the fixed HMIs concentration (10 mg/L) at pH 7. The removal efficiency increased for all HMIs with increasing adsorbent dose due to the increased availability of adsorption sites and reaches equilibrium (0.2 g/L for Pb(II) and Ni(II) and 0.15 g/L for Cd(II)). On the other hand, the q_e decreased for all HMIs with increasing doses. This may be due to the scarcity of HMIs compared to the available binding sites at a higher adsorbent dose [44]. For further experiments, a 0.2 g/L adsorbent dose was used as the optimum dose.

3.2.2. Adsorption kinetics of the single and ternary metal ion systems

The kinetic study was beneficial to understand the adsorption mechanism and determine the adsorption equilibrium time [45,46]. The q_e dependence on contact time is shown in Fig. 7. Initially, a rapid adsorption of HMIs was observed because of vacant adsorbent sites and the strong attraction between HMIs and the MNP-PAMAM surface [8]. In the single HMIs system, the adsorption curve attain equilibrium after 90 min for Pb(II) and Ni(II) HMIs and after 70 min for Cd(II). However, in the ternary HMIs system, the adsorption curve attains equilibrium after 60, 70, and 50 min for Pb(II), Ni(II), and Cd(II) HMIs, respectively. For further experiments, 90 min and 70 min were used as the optimum contact time for the single and ternary system, respectively. In the ternary HMIs system, the strong competition between the coexisting HMIs hinders the interaction between HMIs and available binding sites. Due to this, the q_e for the ternary HMIs system are lower than those for the single systems.

The adsorption kinetics of HMIs onto MNP-PAMAM were analyzed by applying pseudo-first-order (PFO) and pseudo-second-order (PSO) kinetic models. The nonlinear form of the PFO [47] and PSO [48] kinetic model are expressed as,

$$q_t = q_e - q_e e^{-k_1 t} \tag{3}$$

$$q_t = \frac{k_2 q_e^2 t}{1 + k_2 q_e t} \tag{4}$$

where q_e (mg/g), q_t (mg/g), k_1 (min^{-1}), and k_2 (g/mg/min) are the adsorption capacity at equilibrium, the adsorption capacity at time t (min), the rate constants for PFO adsorption, and the rate constants PSO adsorption, respectively. The experimental data fitted with the PFO and PSO kinetic models are shown in Fig. 7(A-C). The kinetic parameters obtained from fitting are listed in Table 1. For single and ternary

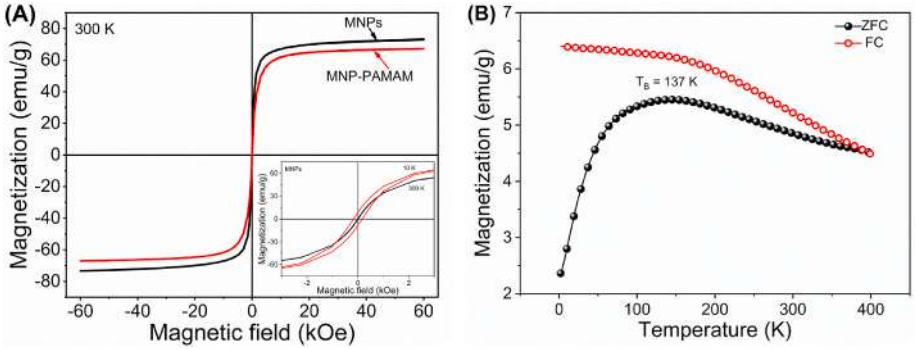

Fig. 5. (A) Saturation magnetization curves of MNPs (black) and MNP-PAMAM (red) measured at 300 K, with the inset showing the MNPs low field magnetization curves emphasizing the increase in the coercive field at 10 K compared to 300 K. (B) Zero field cooled (ZFC) and field cooled (FC) curves of MNPs with a clear phase transition.

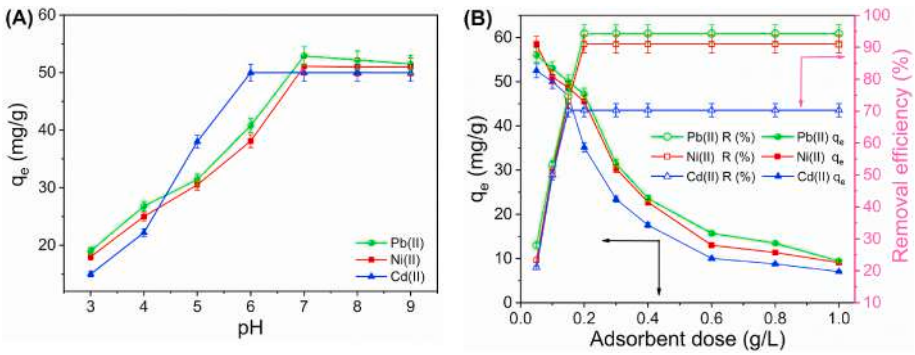

Fig. 6. (A). Effect of pH on the q_e of the MNP-PAMAM nanoadsorbents for Pb(II), Ni(II), and Cd(II) metal ions. (Initial concentration = 10 mg/L, adsorbent dose = 0.1 g/L, and contact time = 60 min). (B) Effect of adsorbent dose on the R % and q_e of Pb(II), Ni(II), and Cd(II) metal ions onto the MNP-PAMAM. (pH = 7, Initial concentration = 10 mg/L, and contact time = 60 min).

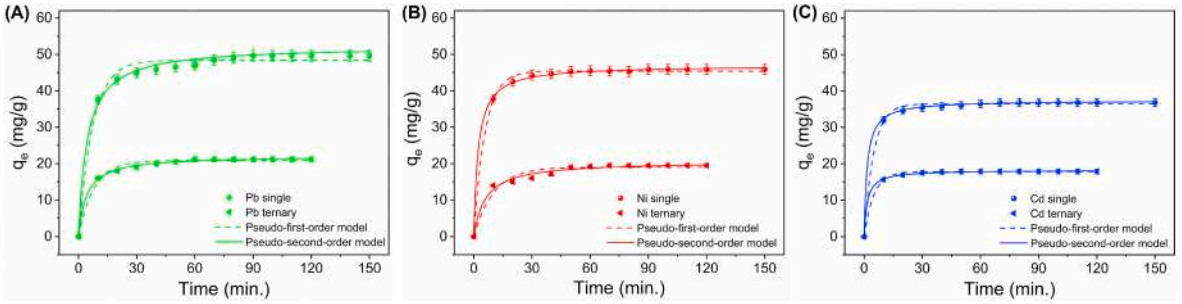

Fig. 7. Influence of the contact time on the q_e of MNP-PAMAM nanoadsorbents and adsorption kinetics for (A) Pb(II), (B) Ni(II), and (C) Cd(II) in the single and ternary metal ion systems (Initial concentration = 10 mg/L, adsorbent dose = 0.2 g/L, and pH = 7).

Table 1
Parameters of the kinetic models for the adsorption of Pb(II), Cd(II), and Ni(II) metal ions on MNP-PAMAM nanoadsorbents in single and ternary systems.

Metal ions	q_e (exp.) (mg/g)	Pseudo-first-order (PFO)			Pseudo-second-order (PSO)		
		q_e (cal.) (mg/g)	k_1 (/min)	R^2	q_e (cal.) (mg/g)	k_2 (g/mg/min)	R^2
Pb(II) single	49.62	48.37	0.135	0.9838	52.29	0.00432	0.9855
Ni(II) single	45.9	45.41	0.17	0.9973	46.99	0.00938	0.9992
Cd(II) single	36.81	36.41	0.2027	0.9865	37.38	0.01758	0.9903
Pb(II) ternary	21.20	20.82	0.1265	0.9842	22.13	0.011	0.9976
Ni(II) ternary	19.51	19.01	0.0976	0.9555	20.62	0.00807	0.9842
Cd(II) ternary	14.50	14.17	0.089	0.9779	15.39	0.00981	0.9966

Note: q_e(exp.) and q_e(cal.) are the equilibrium experimental and calculated adsorption capacities at time t, respectively. R^2 is correlation coefficient.

systems, the values of R^2 for the PFO kinetic model are ($0.9838 < R^2 < 0.9973$) and ($0.9555 < R^2 < 0.9842$), respectively. Whereas, for the PSO model, the R^2 values are ($0.9855 < R^2 < 0.9992$) and ($0.9842 < R^2 < 0.9976$), respectively. Thus, for both HMIs systems, the values of R^2 for the PSO model are higher than the PFO model. This implies that the adsorption follows the PSO model and the overall adsorption is controlled by chemisorption [49].

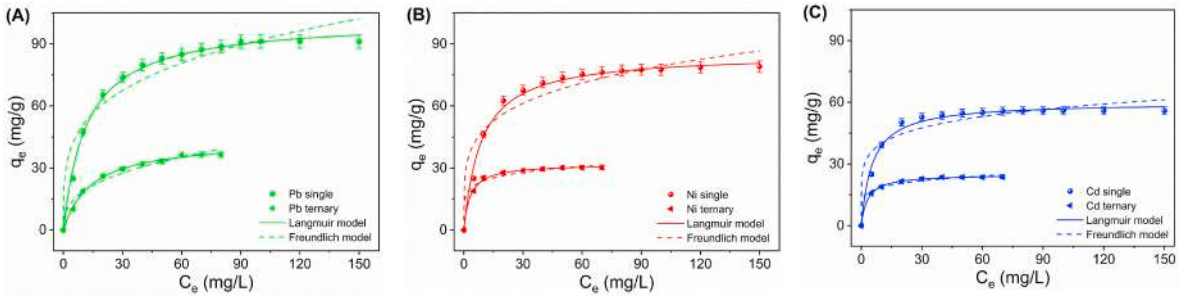

Fig. 8. Effect of the initial concentration of HMIs on the q_e of MNP-PAMAM nanoadsorbents and adsorption isotherm for (A) Pb(II), (B) Ni(II), and (C) Cd(II) in the single and ternary system (pH = 7, adsorbent dose = 0.2 g/L, and contact time = 120 min for single and 70 min for ternary system).

3.2.3. Adsorption isotherms of single and ternary metal ion systems

Adsorption isotherm models help to reveal the surface properties and how HMIs interact with the surface of nanoadsorbents [41]. The Langmuir and Freundlich isotherm models were applied to estimate the maximum q_e of the nanoadsorbent in single and ternary HMIs systems. The equilibrium q_e at different initial HMIs concentrations are shown in Fig. 8. The concentrations were varied from 5 to 150 mg/L for single and 5–80 mg/L for the ternary HMIs system. At the lower concentrations, fewer metal ions are available to adsorb, and consequently, q_e have smaller values. With an increase in HMIs concentration, progressively more ions get adsorbed so that the q_e increases. However, after a certain initial concentration of the HMIs, the q_e reaches equilibrium when all the adsorption sites are occupied.

The nonlinear form of the Langmuir model is expressed as [50],

$$q_e = \frac{K_L q_m C_e}{1 + K_L C_e} \quad (5)$$

'where, q_m is the maximum capacity of adsorbent (mg/g) and K_L is the Langmuir adsorption constant (L/mg). The Langmuir model assumes the homogenous monolayer adsorption between the adsorbates and adsorbents with a finite number of adsorption sites [51,52]. The possibility of the adsorption was decided by separation factor R_L, which is expressed by [53],

$$R_L = \frac{1}{1 + K_L C_0} \quad (6)$$

The nonlinear form of the Freundlich model is expressed as [54],

$$q_e = K_F C_e^{\frac{1}{n}} \quad (7)$$

where, K_F and n are Freundlich constants related to q_e (L/g) and heterogeneity factor (mg/g), respectively. The Freundlich isotherm model is based on the hypothesis of multilayer adsorption of adsorbate on the heterogeneous surface of adsorbents [51]. It also assumes that the number of adsorption sites is not constant. The Langmuir and Freundlich models were applied to experimental data of single and ternary HMIs systems (Fig. 8). The isotherm parameters and constants extracted are reported in Table 2.

From Table 2, for both single and ternary systems, the values of R^2 for the Langmuir model are higher than those for Freundlich model. Also, the q_e calculated by the Langmuir model is well matched to the experimental q_e for both single and ternary HMIs systems. Thus the adsorption process is best fitted to the Langmuir model for both the systems. This indicates that the monolayer adsorption of HMIs onto a homogeneous MNP-PAMAM nanoadsorbents surface. The separation factor R_L lies between 0 and 1 for all HMIs suggesting that the adsorption process is favourable. According to the Langmuir model, maximum adsorption capacities (q_m) of MNP-PAMAM adsorbent for Pb (II), Ni(II), and Cd(II) were 92.82, 80.10, and 57.72 mg/g, respectively, in the single HMIs system. The q_m are compared with previously reported values of other adsorbents and shown in Table 3. For simultaneous removal in the ternary HMIs system, the q_e for Pb (II), Ni(II) and, Cd(II) decreased to 37.00, 31.92, and 24.94 mg/g, respectively. The decrease in q_e for the ternary system is due to the strong competition between different HMIs for acquiring binding sites [41]. The order of the q_e of MNP-PAMAM for both single and ternary systems was found to be Pb(II) > Ni(II) > Cd(II). This can be explained in terms of hydration radius and electronegativity in the single and ternary adsorption processes. The hydrated radius of Pb (II) (4.01 nm) is smaller than that of Ni(II) (4.04 nm) and Cd(II) (4.26 nm). The HMIs with a smaller hydrated radius have higher adsorption affinity due to the smaller diffusion resistance [55,56]. On the other hand, the higher electronegativity of the HMIs leads to a strong affinity to the binding sites of the nanoadsorbent. The electronegativity of Pb(II) (2.33) is higher than that of Ni(II) (1.91) and Cd(II) (1.69) [56,57]. Therefore the q_e for Pb(II) is higher in both systems.

To understand the adsorption mechanism of HMIs on MNP-PAMAM nanoadsorbent, the XPS measurements of nanoadsorbents after adsorption with HMIs were performed. The adsorption of HMIs was confirmed by XPS analysis. The XPS survey spectra of MNP-PAMAM after adsorption of HMIs (Fig. S4A) shows new peaks corresponding to Pb(II), Ni(II), and Cd(II) at binding energies 139.7 eV, 847 eV, and 412 eV, respectively. The Ni (II) peak overlaps with Fe2p peak. The XPS survey spectra of nanoadsorbent loaded with HMIs indicates the Pb(II),

Table 3
Comparison of the adsorption capacities of MNP-PAMAM nanoadsorbents with adsorbents reported in the literature for the removal of Pb (II), Ni(II), and Cd(II) metal ions.

Adsorbent	Adsorption capacity for heavy metal ions (HMIs) (mg/g)			Reference
	Pb (II)	Ni(II)	Cd (II)	
NH_2 functionalized magnetic graphene composite	27.95	22.07	27.83	[58]
Carboxymethyl- cyclodextrin polymer grafted on Fe_3O_4	64.5	13.2	27.7	[59]
OP/Fe_3O_4 magnetic composite	54.94	51.81	–	[60]
Fe_3O_4@C@functional acidic groups	90.7	–	39.7	[61]
PAMAM-grafted chitosan	58.5	–	–	[62]
G2-MCD	49.76	–	–	[63]
G1-NH2-MD	63.63	–	–	[64]
Fe_3O_4@MPTMS	35	–	–	[65]
Amino-functionalized Fe_3O_4 magnetic nano-particles	40.1	–	–	[66]
Sodium dodecyl sulfate-coated magnetite nanoparticles	–	41.2	–	[67]
Polypyrrole functionalized Fe_3O_4 nanoparticle	–	19.92	–	[68]
3-Mercaptopropionic acid functionalized Fe_3O_4 nanoparticles	–	42.01	–	[69]
Carboxyl-modified Fe_3O_4@SiO_2 nanoparticles	–	63.99	–	[70]
Shellac-coated Iron Oxide	–	–	18.8	[71]
Magnetic chitosan nanoparticles	–	–	36.42	[72]
MNP-PAMAM	92.8	80.1	57.72	**Present work**

Table 2
Parameters of the adsorption isotherm model for the adsorption of Pb(II), Cd(II), and Ni(II) metal ions on MNP-PAMAM nanoadsorbents in single and ternary metal ion systems.

Metal ions	q_e (exp.) (mg/g)	Langmuir model			Freundlich model		
		q_m (cal.) (mg/g)	K_L (L/mg)	R^2	K_F (L/mg)	n	R^2
Pb(II) Single	91.16	92.82	0.0842	0.9950	28.11	3.883	0.9316
Ni(II) single	79.017	80.10	0.1138	0.9898	47.54	4.64	0.9150
Cd(II) single	56.11	57.72	0.1836	0.9883	27.9	6.37	0.92
Pb(II) ternary	36.46	37.00	0.0707	0.9965	8.16	2.79	0.9671
Ni(II) ternary	30.80	31.92	0.3218	0.9972	17.041	6.89	0.9786
Cd(II) ternary	23.61	24.94	0.3285	0.9990	13.41	6.95	0.9862

Note: q_e(exp.) and q_m(cal.) are the experimental and calculated adsorption capacity, respectively. R^2 is correlation coefficient.

Ni(II), and Cd(II) adsorption on the surface of the MNP-PAMAM. The high-resolution spectra of adsorbed Pb(II) metal ions (Fig. S4B) show two peaks corresponding to Pb4f$_{7/2}$ (138.1 eV) and Pb4f$_{5/2}$ (142.9 eV) indicating formation of bidentate complex on the surface of MNP-PAMAM [73]. The high-resolution XPS spectra of Ni(II) loaded on the nanoadsorbent (Fig. S4C) shows two peaks viz. Ni 2p$_{3/2}$ and Ni 2p$_{1/2}$. The Ni 2p$_{3/2}$ peak was deconvoluted into two peaks at binding energies 856.2 eV (Ni 2p$_{3/2}$) and 862.4 eV (Ni 2p$_{3/2}$ satellite). Also, the Ni 2p$_{1/2}$ peak was deconvoluted into two peaks at binding energies 874.8 eV (Ni 2p$_{1/2}$) and 879.6 eV (Ni 2p$_{1/2}$ satellite) [74]. The high-resolution spectra of Cd (II) (Fig. S4D) indicate two peaks corresponding to Cd3d$_{5/2}$ (404.9 eV) and Cd3d$_{3/2}$ (412.1 eV) which shows the Cd(II) was adsorbed on the MNP-PAMAM surface [75]. Cd(II) and Ni(II) are complexed with N atom of nanoadsorbents by providing a lone pair of electrons to form a covalent bond [73]. Thus high-resolution XPS spectra of metal ions confirms that metal ions were adsorbed on the MNP-PAMAM nanoadsorbent surface through chemisorption.

3.3. Desorption and reusability study

The reusability study (Fig. 9) revealed that after five consecutive adsorption/desorption cycles, the efficiency of Pb(II), Ni(II), and Cd(II) decreased by 16, 17, and 21%, respectively, as compared to the original removal efficiency. The results demonstrate that the MNP-PAMAM nanoadsorbents have good regeneration performance and can be reused as effective nanoadsorbents to remove HMIs from water.

4. Conclusions

To provide a high density of functional groups to MNPs for the simultaneous removal of coexisting HMIs, MNPs were modified with second-generation amino terminated PAMAM dendrimer. Before dendritic modification, a novel approach of recrystallization of MNPs for the removal of OA/OM moieties on the surface of MNPs was used. The XRD and TEM analysis showed that the spherical-shaped MNPs have a pure magnetite phase with an average particle size of 8.6 ± 1.5 nm. FTIR and XPS investigations confirmed the successful grafting of the PAMAM dendrimer on the surface of MNPs. Magnetic measurement of MNPs (M_s = 69 emu/g) and MNP-PAMAM (M_s = 64 emu/g) revealed their superparamagnetic nature at RT. The grafting percentage calculated from magnetization data of PAMAM dendrimer on the MNPs nanoadsorbent surface was around 7.24 wt %. BET analysis showed that the surface area of MNP-PAMAM (111 m^2/g) was increased compared to that of as prepared MNPs (75 m^2/g). The zeta potential study verified good colloidal stability due to electrostatic repulsion among the MNP-PAMAM nanoadsorbents. The MNP-PAMAM nanoadsorbents were successfully employed for the individual and simultaneous removal of Pb (II), Ni(II), and Cd(II) ions from the aqueous solution. The q_m for the simultaneous removal of Pb(II), Ni(II), and Cd(II) in the ternary system were found to be 37.00, 31.92, and 24.94 mg/g, respectively. In single systems, the q_m for Pb(II), Ni(II), and Cd(II) were increased to 92.82, 80.10, and 57.72 mg/g, respectively. The kinetic studies indicate that adsorption data in single and ternary HMIs systems best fit the PSO kinetic model. This suggests that the chemisorption process is mediated by the active amino groups on the surface of MNP-PAMAM. In both the single and ternary systems, the experimental data were modelled by the Langmuir adsorption model, which suggests homogeneous monolayer adsorption between the surface of nanoadsorbent and HMIs. In both single and ternary systems, the order of the q_e of nanoadsorbent was found to be Pb(II) > Ni(II) > Cd(II). The MNP-PAMAM showed excellent regeneration performance up to five adsorption/desorption cycles. Thus, the hyperbranched MNP-PAMAM nanoadsorbents have promising potential for efficiently removing coexisting multiple HMIs from aqueous solutions.

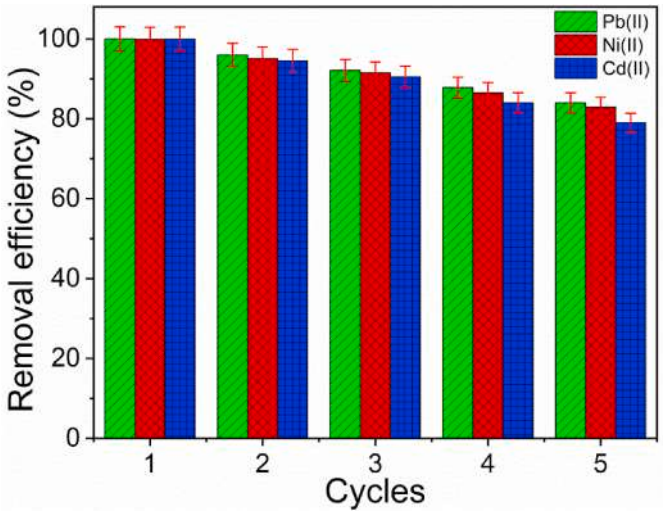

Fig. 9. Reusability of MNP-PAMAM nanoadsorbents for adsorption/desorption of Pb(II), Ni(II), and Cd(II) metal ions.

CRediT authorship contribution statement

V.P. Kothavale: Data curation, Writing – original draft. **A. Sharma:** Data curation, Writing – original draft, Materials characterization. **R.P. Dhavale:** Materials characterization. **V.D. Chavan:** Data curation, Writing – original draft. **S.R. Shingte:** Data curation, Writing – original draft. **O. Selyshchev:** Materials characterization. **T.D. Dongale:** Materials characterization. **H.H. Park:** Writing – review & editing. **D.R.T. Zahn:** Writing – review & editing. **G. Salvan:** Writing – review & editing. **P.B. Patil:** Conceptualization, Methodology, experimental, Supervision, Writing – review & editing, Writing – original draft, draft revision.

Declaration of competing interest

The authors declare that they have no known competing financial interests or personal relationships that could have appeared to influence the work reported in this paper.

Data availability

Data will be made available on request.

Acknowledgements

P.B. Patil would like to acknowledge the Science and Engineering Research Board, Department of Science and Technology (DST-SERB), Government of India for financial support (No. EMR/2017/001810). A. Sharma and G. Salvan acknowledge the financial support provided by the Deutsche Forschungsgemeinschaft (DFG) under project number 282193534. R.P. Dhavale and H.H. Park would like to acknowledge that this work is supported by the National Research Foundation of Korea (NRF) grant funded by the Korean government (MSIT) (No. 2020R1A5A1019131).

Appendix A. Supplementary data

Supplementary data to this article can be found online at https://doi.org/10.1016/j.matchemphys.2022.126792.

References

[1] F. Di Natale, A. Erto, A. Lancia, Desorption of arsenic from exhaust activated carbons used for water purification, J. Hazard Mater. 260 (2013) 451–458, https://doi.org/10.1016/j.jhazmat.2013.05.055.

[2] R. Apiratikul, P. Pavasant, Batch and column studies of biosorption of heavy metals by Caulerpa lentillifera, Bioresour. Technol. 99 (2008) 2766–2777, https://doi.org/10.1016/j.biortech.2007.06.036.

[3] K. Rida, S. Bouraoui, S. Hadnine, Adsorption of methylene blue from aqueous solution by kaolin and zeolite, Appl. Clay Sci. (2013) 83–84, https://doi.org/10.1016/j.clay.2013.08.015, 99–105.

[4] W. Peng, H. Li, Y. Liu, S. Song, A review on heavy metal ions adsorption from water by graphene oxide and its composites, J. Mol. Liq. 230 (2017) 496–504, https://doi.org/10.1016/j.molliq.2017.01.064.

[5] S.C.N. Tang, I.M.C. Lo, Magnetic nanoparticles: essential factors for sustainable environmental applications, Water Res. 47 (2013) 2613–2632, https://doi.org/10.1016/j.watres.2013.02.039.

[6] S.-H. Huang, D.-H. Chen, Rapid removal of heavy metal cations and anions from aqueous solutions by an amino-functionalized magnetic nano-adsorbent, J. Hazard Mater. 163 (2009) 174–179, https://doi.org/10.1016/j.jhazmat.2008.06.075.

[7] P.P. Waifalkar, S.B. Parit, A.D. Chougale, S.C. Sahoo, P.S. Patil, P.B. Patil, Immobilization of invertase on chitosan coated γ-Fe_2O_3 magnetic nanoparticles to facilitate magnetic separation, J. Colloid Interface Sci. 482 (2016) 159–164, https://doi.org/10.1016/j.jcis.2016.07.082.

[8] V.D. Chavan, V.P. Kothavale, S.C. Sahoo, P. Kollu, T.D. Dongale, P.S. Patil, P. B. Patil, Adsorption and kinetic behavior of Cu(II) ions from aqueous solution on DMSA functionalized magnetic nanoparticles, Phys. B Condens. Matter 571 (2019) 273–279, https://doi.org/10.1016/j.physb.2019.07.026.

[9] W. Yantasee, C.L. Warner, T. Sangvanich, R.S. Addleman, T.G. Carter, R.J. Wiacek, G.E. Fryxell, C. Timchalk, M.G. Warner, Removal of heavy metals from aqueous systems with thiol functionalized superparamagnetic nanoparticles, Environ. Sci. Technol. 41 (2007) 5114–5119, https://doi.org/10.1021/es0705238.

[10] S.S. Banerjee, D.-H. Chen, Fast removal of copper ions by gum Arabic modified magnetic nano-adsorbent, J. Hazard Mater. 147 (2007) 792–799, https://doi.org/10.1016/j.jhazmat.2007.01.079.

[11] V.P. Kothavale, V.C. Karade, P.P. Waifalkar, S.C. Sahoo, P.S. Patil, P.B. Patil, Removal of Cu(II) metal ions from aqueous solution by amine functionalized magnetic nanoparticles, AIP Conf. Proc. (2018), 050038, https://doi.org/10.1063/1.5028669.

[12] V.P. Kothavale, V.D. Chavan, S.C. Sahoo, P. Kollu, T.D. Dongale, P.S. Patil, P. B. Patil, Removal of Cu(II) from aqueous solution using APTES-GA modified magnetic iron oxide nanoparticles: kinetic and isotherm study, Mater. Res. Express 6 (2019), 106103, https://doi.org/10.1088/2053-1591/ab3590.

[13] J.-Y. Tseng, C.-Y. Chang, C.-F. Chang, Y.-H. Chen, C.-C. Chang, D.-R. Ji, C.-Y. Chiu, P.-C. Chiang, Kinetics and equilibrium of desorption removal of copper from magnetic polymer adsorbent, J. Hazard Mater. 171 (2009) 370–377, https://doi.org/10.1016/j.jhazmat.2009.06.030.

[14] Y. Wu, C. Chen, Q. Zhou, Q.X. Li, Y. Yuan, Y. Tong, H. Wang, X. Zhou, Y. Sun, X. Sheng, Polyamidoamine dendrimer decorated nanoparticles as an adsorbent for magnetic solid-phase extraction of tetrabromobisphenol A and 4-nonylphenol from environmental water samples, J. Colloid Interface Sci. 539 (2019) 361–369, https://doi.org/10.1016/j.jcis.2018.12.064.

[15] A. Ali, T. Shah, R. Ullah, P. Zhou, M. Guo, M. Ovais, Z. Tan, Y. Rui, Review on recent progress in magnetic nanoparticles: synthesis, characterization, and diverse applications, Front. Chem. 9 (2021) 548, https://doi.org/10.3389/fchem.2021.629054.

[16] R. Khodadust, G. Unsoy, S. Yalcın, G. Gunduz, U. Gunduz, PAMAM dendrimer-coated iron oxide nanoparticles: synthesis and characterization of different generations, J. Nanoparticle Res. 15 (2013) 1488, https://doi.org/10.1007/s11051-013-1488-6.

[17] Y. Zhou, L. Luan, B. Tang, Y. Niu, R. Qu, Y. Liu, W. Xu, Fabrication of Schiff base decorated PAMAM dendrimer/magnetic Fe_3O_4 for selective removal of aqueous Hg (II), Chem. Eng. J. 398 (2020), 125651, https://doi.org/10.1016/j.cej.2020.125651.

[18] L. Luan, B. Tang, Y. Liu, A. Wang, B. Zhang, W. Xu, Y. Niu, Selective capture of Hg (II) and Ag(I) from water by sulfur-functionalized polyamidoamine dendrimer/magnetic Fe_3O_4 hybrid materials, Separ. Purif. Technol. 257 (2021), 117902, https://doi.org/10.1016/j.seppur.2020.117902.

[19] R.P. Dhavale, P.P. Waifalkar, A. Sharma, R.P. Dhavale, S.C. Sahoo, P. Kollu, A. D. Chougale, D.R.T. Zahn, G. Salvan, P.S. Patil, P.B. Patil, Monolayer grafting of aminosilane on magnetic nanoparticles: an efficient approach for targeted drug delivery system, J. Colloid Interface Sci. 529 (2018) 415–425, https://doi.org/10.1016/j.jcis.2018.06.006.

[20] S. Sun, H. Zeng, D.B. Robinson, S. Raoux, P.M. Rice, S.X. Wang, G. Li, Monodisperse MFe_2O_4 (M = Fe, Co, Mn) nanoparticles, J. Am. Chem. Soc. 126 (2004) 273–279, https://doi.org/10.1021/ja0380852.

[21] R. Chen, M.G. Christiansen, P. Anikeeva, Maximizing hysteretic losses in magnetic ferrite nanoparticles via model-driven synthesis and materials optimization, ACS Nano 7 (2013) 8990–9000, https://doi.org/10.1021/nn4035266.

[22] O. Bixner, A. Lassenberger, D. Baurecht, E. Reimhult, Complete exchange of the hydrophobic dispersant shell on monodisperse superparamagnetic iron oxide nanoparticles, Langmuir 31 (2015) 9198–9204, https://doi.org/10.1021/acs.langmuir.5b01833.

[23] V.C. Karade, A. Sharma, R.P. Dhavale, R.P. Dhavale, S.R. Shingte, P.S. Patil, J. H. Kim, D.R.T. Zahn, A.D. Chougale, G. Salvan, P.B. Patil, APTES monolayer coverage on self-assembled magnetic nanospheres for controlled release of anticancer drug Nintedanib, Sci. Rep. 11 (2021) 5674, https://doi.org/10.1038/s41598-021-84770-0.

[24] K.J. Kim, J.W. Park, Stability and reusability of amine-functionalized magnetic-cored dendrimer for heavy metal adsorption, J. Mater. Sci. 52 (2017) 843–857, https://doi.org/10.1007/s10853-016-0380-z.

[25] B. Pan, D. Cui, Y. Sheng, C. Ozkan, F. Gao, R. He, Q. Li, P. Xu, T. Huang, Dendrimer-modified magnetic nanoparticles enhance efficiency of gene delivery system, Cancer Res. 67 (2007) 8156–8163, https://doi.org/10.1158/0008-5472.CAN-06-4762.

[26] Y. Waseda, E. Matsubara, K. Shinoda, X-Ray Diffraction Crystallography, Springer Berlin Heidelberg, Berlin, Heidelberg, 2011, https://doi.org/10.1007/978-3-642-16635-8.

[27] D. Maity, S. Choo, J. Yi, J.D. Ã, J.M.X. Ã, Synthesis of magnetite nanoparticles via a solvent-free thermal decomposition route, J. Magn. Magn Mater. 321 (2009) 1256–1259, https://doi.org/10.1016/j.jmmm.2008.11.013.

[28] L. Zhang, R. He, H.C. Gu, Oleic acid coating on the monodisperse magnetite nanoparticles, Appl. Surf. Sci. 253 (2006) 2611–2617, https://doi.org/10.1016/j.apsusc.2006.05.023.

[29] H. Sharifi Dehsari, R.A. Harris, A.H. Ribeiro, W. Tremel, K. Asadi, Optimizing the binding energy of the surfactant to iron oxide yields truly monodisperse nanoparticles, Langmuir 34 (2018) 6582–6590, https://doi.org/10.1021/acs.langmuir.8b01337.

[30] T.K.O. Vuong, D.L. Tran, T.L. Le, D.V. Pham, H.N. Pham, T.H. Le Ngo, H.M. Do, X. P. Nguyen, Synthesis of high-magnetization and monodisperse Fe_3O_4 nanoparticles via thermal decomposition, Mater. Chem. Phys. 163 (2015) 537–544, https://doi.org/10.1016/j.matchemphys.2015.08.010.

[31] Y. Wang, P. Su, S. Wang, J. Wu, J. Huang, Y. Yang, Dendrimer modified magnetic nanoparticles for immobilized BSA: a novel chiral magnetic nano-selector for direct separation of racemates, J. Mater. Chem. B. 1 (2013) 5028–5035, https://doi.org/10.1039/c3tb20889c.

[32] M. Salimi, S. Sarkar, R. Saber, H. Delavari, A.M. Alizadeh, H.T. Mulder, Magnetic hyperthermia of breast cancer cells and MRI relaxometry with dendrimer-coated iron-oxide nanoparticles, Cancer Nanotechnol. 9 (2018) 7, https://doi.org/10.1186/s12645-018-0042-8.

[33] X. Qian Tang, Y. Dan Zhang, Z. Wei Jiang, D. Mei Wang, C. Zhi Huang, Y. Fang Li, Fe_3O_4 and metal–organic framework MIL-101(Fe) composites catalyze luminol chemiluminescence for sensitively sensing hydrogen peroxide and glucose, Talanta 179 (2018) 43–50, https://doi.org/10.1016/j.talanta.2017.10.049.

[34] C. Koo, H. Hong, P.W. Im, H. Kim, C. Lee, X. Jin, B. Yan, W. Lee, H.-J. Im, S. H. Paek, Y. Piao, Magnetic and near-infrared derived heating characteristics of dimercaptosuccinic acid coated uniform Fe@Fe_3O_4 core–shell nanoparticles, Nano Converg. 7 (2020) 20, https://doi.org/10.1186/s40580-020-00229-4.

[35] T. Wang, W.L. Yang, Y. Hong, Y.L. Hou, Magnetic nanoparticles grafted with amino-riched dendrimer as magnetic flocculant for efficient harvesting of oleaginous microalgae, Chem. Eng. J. 297 (2016) 304–314, https://doi.org/10.1016/j.cej.2016.03.038.

[36] D. Yimin, L. Danyang, Z. Jiaqi, W. Shengyun, Z. Yi, Facile preparation of amidoxime-functionalized Fe_3O_4@SiO_2-: G -PAMAM-AO magnetic composites for enhanced adsorption of Pb(II) and Ni(II) from aqueous solution, RSC Adv. 9 (2019) 9171–9179, https://doi.org/10.1039/c9ra00128j.

[37] A. Sharma, A.D. Chougale, G. Salvan, P.B. Patil, Chapter 15. Magnetoresistance-Based biosensors, in: M.H. Chaudhery (Ed.), Anal. Appl. Funct. Magn. Nanoparticles, Royal Society of Chemistry, Cambridge, 2021, pp. 369–396, https://doi.org/10.1039/9781839162756-00369.

[38] Y. Tan, Z. Zhuang, Q. Peng, Y. Li, Room-temperature soft magnetic iron oxide nanocrystals: synthesis, characterization, and size-dependent magnetic properties, Chem. Mater. 20 (2008) 5029–5034, https://doi.org/10.1021/cm801082p.

[39] V. Kumar, R.P. Singh, S. Kumar, A. Agarwal, P. Singh, Particle size determination and magnetic characterization of Fe_3O_4 nanoparticles using superconducting quantum interference device magnetometry, Sensor. Mater. 28 (2016) 191–199, https://doi.org/10.18494/SAM.2016.1169.

[40] M. Banaei, M. Salami-Kalajahi, A “grafting to” approach to synthesize low cytotoxic poly(aminoamide)-dendrimer-grafted Fe_3O_4 magnetic nanoparticles, Adv. Polym. Technol. 37 (2018) 943–948, https://doi.org/10.1002/adv.21741.

[41] L. Zhang, J. Guo, X. Huang, W. Wang, P. Sun, Y. Li, J. Han, Functionalized biochar-supported magnetic $MnFe_2O_4$ nanocomposite for the removal of Pb(ii) and Cd(ii), RSC Adv. 9 (2019) 365–376, https://doi.org/10.1039/c8ra09061k.

[42] Y.M. Hao, C. Man, Z.B. Hu, Effective removal of Cu (II) ions from aqueous solution by amino-functionalized magnetic nanoparticles, J. Hazard Mater. 184 (2010) 392–399, https://doi.org/10.1016/j.jhazmat.2010.08.048.

[43] B. Ren, K. Wang, B. Zhang, H. Li, Y. Niu, H. Chen, Z. Yang, X. Li, H. Zhang, Adsorption behavior of PAMAM dendrimers functionalized silica for Cd(II) from aqueous solution: experimental and theoretical calculation, J. Taiwan Inst. Chem. Eng. 101 (2019) 80–91, https://doi.org/10.1016/j.jtice.2019.04.037.

[44] V. Javanbakht, S.M. Ghoreishi, N. Habibi, M. Javanbakht, A novel magnetic chitosan/clinoptilolite/magnetite nanocomposite for highly efficient removal of Pb (II) ions from aqueous solution, Powder Technol. 302 (2016) 372–383, https://doi.org/10.1016/j.powtec.2016.08.069.

[45] P. Tan, J. Wen, Y. Hu, X. Tan, Adsorption of Cu^{2+} and Cd^{2+} from aqueous solution by novel electrospun poly(vinyl alcohol)/graphene oxide nanofibers, RSC Adv. 6 (2016) 79641–79650, https://doi.org/10.1039/c6ra18052c.

[46] M. Liu, B. Zhang, H. Wang, F. Zhao, Y. Chen, Q. Sun, Facile crosslinking synthesis of hyperbranch-substrate nanonetwork magnetite nanocomposite for the fast and highly efficient removal of lead ions and anionic dyes from aqueous solutions, RSC Adv. 6 (2016) 67057–67071, https://doi.org/10.1039/c6ra11037a.

[47] H. Yuh-Shan, Citation review of Lagergren kinetic rate equation on adsorption reactions, Scientometrics 59 (2004) 171–177, https://doi.org/10.1023/B:SCIE.0000013305.99473.cf.
[48] Y.S. Ho, G. McKay, Pseudo-second order model for sorption processes, Process Biochem. 34 (1999) 451–465, https://doi.org/10.1016/S0032-9592(98)00112-5.
[49] D. Singh, R.K. Gautam, R. Kumar, B.K. Shukla, V. Shankar, V. Krishna, Citric acid coated magnetic nanoparticles: synthesis, characterization and application in removal of Cd(II) ions from aqueous solution, J. Water Proc. Eng. 4 (2014) 233–241, https://doi.org/10.1016/j.jwpe.2014.10.005.
[50] I. Langmuir, Adsorption of gases on plain surfaces of glass mica platinum, J. Am. Chem. Soc. 40 (1918) 1361–1403, https://doi.org/10.1006/ceps.2001.1094.
[51] N. Tang, C.-G. Niu, X.-T. Li, C. Liang, H. Guo, L.-S. Lin, C.-W. Zheng, G.-M. Zeng, Efficient removal of Cd^{2+} and Pb^{2+} from aqueous solution with amino- and thiol-functionalized activated carbon: isotherm and kinetics modeling, Sci. Total Environ. 635 (2018) 1331–1344, https://doi.org/10.1016/j.scitotenv.2018.04.236.
[52] X. Zhao, H. Wang, H. Peng, L. Wang, X. Lu, Y. Huang, J. Chen, T. Shao, Buoyant ALG/HA/HGMs composite adsorbents for highly efficient removal of copper from aqueous solution and contaminated kaolin soil, Chem. Eng. J. 327 (2017) 244–256, https://doi.org/10.1016/j.cej.2017.06.085.
[53] K.R. Hall, L.C. Eagleton, A. Acrivos, T. Vermeulen, Pore- and solid-diffusion kinetics in fixed-bed adsorption under constant-pattern conditions, Ind. Eng. Chem. Fundam. 5 (2002) 212–223, https://doi.org/10.1021/i160018a011.
[54] A.H. Chen, C.Y. Yang, C.Y. Chen, C.Y. Chen, C.W. Chen, The chemically crosslinked metal-complexed chitosans for comparative adsorptions of Cu(II), Zn(II), Ni(II) and Pb(II) ions in aqueous medium, J. Hazard Mater. 163 (2009) 1068–1075, https://doi.org/10.1016/j.jhazmat.2008.07.073.
[55] S.B. Chen, Y.B. Ma, L. Chen, K. Xian, Adsorption of aqueous Cd^{2+}, Pb^{2+}, Cu^{2+} ions by nano-hydroxyapatite: single-and multi-metal competitive adsorption study, Geochem. J. 44 (2010) 233–239, https://doi.org/10.2343/geochemj.1.0065.
[56] I. Mobasherpour, E. Salahi, M. Pazouki, Comparative of the removal of Pb^{2+}, Cd^{2+} and Ni^{2+} by nano crystallite hydroxyapatite from aqueous solutions: adsorption isotherm study, Arab. J. Chem. 5 (2012) 439–446, https://doi.org/10.1016/j.arabjc.2010.12.022.
[57] J. Bayo, Kinetic studies for Cd(II) biosorption from treated urban effluents by native grapefruit biomass (Citrus paradisi L.): the competitive effect of Pb(II), Cu (II) and Ni(II), Chem. Eng. J. 191 (2012) 278–287, https://doi.org/10.1016/j.cej.2012.03.016.
[58] X. Guo, B. Du, Q. Wei, J. Yang, L. Hu, L. Yan, W. Xu, Synthesis of amino functionalized magnetic graphenes composite material and its application to remove Cr(VI), Pb(II), Hg(II), Cd(II) and Ni(II) from contaminated water, J. Hazard Mater. 278 (2014) 211–220, https://doi.org/10.1016/j.jhazmat.2014.05.075.
[59] A.Z.M. Badruddoza, Z.B.Z. Shawon, W.J.D. Tay, K. Hidajat, M.S. Uddin, Fe_3O_4/cyclodextrin polymer nanocomposites for selective heavy metals removal from industrial wastewater, Carbohydr. Polym. 91 (2013) 322–332, https://doi.org/10.1016/j.carbpol.2012.08.030.
[60] M. Shafiee, R. Foroutan, K. Fouladi, M. Ahmadlouydarab, B. Ramavandi, S. Sahebi, Application of oak powder/Fe_3O_4 magnetic composite in toxic metals removal from aqueous solutions, Adv. Powder Technol. 30 (2019) 544–554, https://doi.org/10.1016/j.apt.2018.12.006.
[61] Z. Chen, Z. Geng, Z. Zhang, L. Ren, T. Tao, R. Yang, Z. Guo, Synthesis of magnetic Fe_3O_4@C nanoparticles modified with -SO_3H and -COOH groups for fast removal of Pb^{2+}, Hg^{2+}, and Cd^{2+} ions, Eur. J. Inorg. Chem. 2014 (2015) 3172–3177, https://doi.org/10.1002/ejic.201301500.
[62] Z. Zarghami, A. Akbari, A.M. Latifi, M.A. Amani, Design of a new integrated chitosan-PAMAM dendrimer biosorbent for heavy metals removing and study of its adsorption kinetics and thermodynamics, Bioresour. Technol. 205 (2016) 230–238, https://doi.org/10.1016/j.biortech.2016.01.052.
[63] S.J. Lee, Y.L. Han, S.J. Park, J.W. Park, Optimal generation number in magnetic-cored dendrimers as Pb(II) and Cd(II) adsorbents, Environ. Technol. (2019) 3330, https://doi.org/10.1080/09593330.2019.1611935.
[64] H.R. Kim, D.W. Boukhvalov, S.J. Lee, J.W. Park, Computational calculation identified optimal binding sites in nano-sized magnetic-cored dendrimer, Chemosphere 210 (2018) 287–295, https://doi.org/10.1016/j.chemosphere.2018.06.174.
[65] S. Villa, P. Riani, F. Soggia, E. Magi, F. Canepa, Thiol-functionalized magnetic nanoparticles for static and dynamic removal of Pb(II) ions from waters, J. Nanoparticle Res. 21 (2019), https://doi.org/10.1007/s11051-019-4482-9.
[66] Y. Tan, M. Chen, Y. Hao, High efficient removal of Pb (II) by amino-functionalized Fe_3O_4 magnetic nano-particles, Chem. Eng. J. 191 (2012) 104–111, https://doi.org/10.1016/j.cej.2012.02.075.
[67] M. Adeli, Y. Yamini, M. Faraji, Removal of copper, nickel and zinc by sodium dodecyl sulphate coated magnetite nanoparticles from water and wastewater samples, Arab. J. Chem. 10 (2017) S514, https://doi.org/10.1016/j.arabjc.2012.10.012. –S521.
[68] K. Chithra, R.T. Akshayaraj, K. Pandian, Polypyrrole-protected magnetic nanoparticles as an excellent sorbent for effective removal of Cr(VI) and Ni(II) from effluent water: kinetic studies and error analysis, Arabian J. Sci. Eng. 43 (2018) 6219–6228, https://doi.org/10.1007/s13369-018-3421-x.
[69] S. Venkateswarlu, S. Himagirish Kumar, N.V.V. Jyothi, Rapid removal of Ni(II) from aqueous solution using 3-Mercaptopropionic acid functionalized bio magnetite nanoparticles, Water Resour. Ind. 12 (2015) 1–7, https://doi.org/10.1016/j.wri.2015.09.001.
[70] S. Ghafoor, S. Ata, Synthesis of Carboxyl-modified Fe_3O_4@SiO_2 nanoparticles and their utilization for the remediation of cadmium and nickel from aqueous solution, J. Chil. Chem. Soc. 62 (2017) 3588–3592, https://doi.org/10.4067/s0717-97072017000303588.
[71] J. Gong, L. Chen, G. Zeng, F. Long, J. Deng, Q. Niu, X. He, Shellac-coated iron oxide nanoparticles for removal of cadmium(II) ions from aqueous solution, J. Environ. Sci. (China). 24 (2012) 1165–1173, https://doi.org/10.1016/S1001-0742(11)60934-0.
[72] H.L. Fan, S.F. Zhou, W.Z. Jiao, G.S. Qi, Y.Z. Liu, Removal of heavy metal ions by magnetic chitosan nanoparticles prepared continuously via high-gravity reactive precipitation method, Carbohydr. Polym. 174 (2017) 1192–1200, https://doi.org/10.1016/j.carbpol.2017.07.050.
[73] W. Qu, D. He, Y. Guo, Y. Tang, J. Shang, L. Zhou, R. Zhu, R.J. Song, Adsorption of Ni^{2+} and Pb^{2+} from water using diethylenetriamine-grafted Spirodela polyrhiza: behavior and mechanism studies, Environ. Sci. Pollut. Res. 26 (2019) 34562–34574, https://doi.org/10.1007/s11356-019-06558-0.
[74] T. Li, W. Zhang, S. Zhai, G. Gao, J. Ding, W. Zhang, Y. Liu, X. Zhao, B. Pan, L. Lv, Efficient removal of nickel(II) from high salinity wastewater by a novel PAA/ZIF-8/PVDF hybrid ultrafiltration membrane, Water Res. 143 (2018) 87–98, https://doi.org/10.1016/j.watres.2018.06.031.
[75] K. Chen, J. He, Y. Li, X. Cai, K. Zhang, T. Liu, Y. Hu, D. Lin, L. Kong, J. Liu, Removal of cadmium and lead ions from water by sulfonated magnetic nanoparticle adsorbents, J. Colloid Interface Sci. 494 (2017) 307–316, https://doi.org/10.1016/j.jcis.2017.01.082.